Sensors & Transducers, Vol. 255, Issue 1, January 2022, pp. 24-34

www.sensorsportal.com

Sensors & Transducers

Published by IFSA Publishing, S. L., 2022
http://www.sensorsportal.com

High Performance InAs/InP Quantum Dash Frequency Comb Laser for High Capacity RoF Wireless Networks

[1, *] Youxin Mao, [1, 2] Khan Zeb, [1] Zhengou Lu, [1] Jiaren Liu, [1] Guocheng Liu, [1] Philip J. Poole, [1] Mohamed Rahim, [1] Grzegorz Pakulski, [1] Pedro Barrios, [1] Weihong Jiang and [2] John Zhang

[1] Advanced Elect. and Photonics Research Centre, National Research Council Canada, Ottawa, ON, Canada

[2] iPhotonics Labs, Dept. of Elect. and Computer Engineering, Concordia University, Montreal, QC, Canada

[*] Tel.: + 613-993-7331

E-mail: youxin.mao@nrc-cnrc.gc.ca

Received: 23 November 2021 /Accepted: 30 December 2021 /Published: 31 January 2022

Abstract: We demonstrate a high performance C-band semiconductor quantum dash (QD) mode-locked laser based optical frequency comb (OFC) with buried heterostructure (BH). Theory of timing jitter is presented including characterization methods from both the 1st homonic RF power spectral density and optical phase noise. Experimental results of relative intensity noise (RIN), phase noise, and timing jitter are compared from QD mode-locked optical frequency comb having BH structure to that with conventional surface ridge structure in the same repetition rate of 25 GHz. It is demonstrated that the laser with BH structure exhibits significantly reduced RIN, phase noise, and timing jitter compared to the surface ridge structure. The performance of BH QD OFC is also evaluated in broadband optical heterodyne based radio-over-fiber fronthaul wireless links at 5G New Radio of around 25 GHz with a total bit rate of 16-Gb/s.

Keywords: Semiconductor quantum dot or dash mode-locked laser, Optical frequency comb, Buried hetero-structure, Phase noise, Timing jitter, Radio-over-fiber, 5G new radio.

1. Introduction

To meet rapidly increased demand for wireless and internet worldwide and to overcome the global shortage of RF bandwidth, high-speed networks and the millimeter-wave (mm-wave) spectra are expected [1] to increase data capacity and the wireless frequency bandwidth. To keep symbol rates compliant with the electrical bandwidth of energy-efficient CMOS driver circuitry, a technical implementation of such networks requires higher-order modulation formats along with parallel transmission on multitude of wavelength channels [2]. In these circumstances, optical frequency combs (OFCs) become particularly attractive light sources to generate large numbers of well-defined carriers for wavelength-division multiplexing (WDM) in a single chip-scale device. Particularly one of the important advantages of CFCs is that the comb lines are inherently equidistance in frequency, hence, easing the requirements for inter-channel guard bands and avoiding frequency control of individual lines as needed in conventional used arrays of independent DFB lasers. These advantages do not only apply to the WDM transmitter but also to

the receiver, where an array of discrete local oscillators (LO) may be replaced by a single CFC [3] and possibly with the same CFC as the transmitter light source.

OFCs generated by monolithic semiconductor mode-locked lasers (MLLs) have been demonstrated to be efficient for WDM based communication networks owing to compact size, low power consumption, wide optical bandwidth with a flat optical spectrum, and the ability for hybrid integration with silicon substrates. It has been demonstrated that using quantum dots or dashes as the active gain medium instead of bulk layers or quantum wells for semiconductor lasers a number of enhancements in device performance were found [4-5]. These include sharp increase in the density of states and reduction in the amount of amplified spontaneous emission rates, which leads to lower intrinsic noise, lower threshold current densities, lower sensitivity of the threshold current to temperature, reduced chirps, broader spectral gain bandwidths, narrower mode linewidth, and faster carrier dynamics. The QD single-section passively (SSP) MLLs or called passively MLLs are more promising OFCs for the next generation of high-speed networks [6-8]. Due to without a saturable absorber section, the SSP MLLs achieve mode-locking results in an increased average output power, simpler fabrication, able to make higher repetition rate [9, 10].

Significant reductions of phase noise and pulse jitter have been reported using active mode-locking [11], hybrid mode-locking [12, 13] and optical injection [14-16] methods in frequency comb QD lasers at 1300 nm wavelength. It is shown that the best suppressing level of time jitter could be down to sub-hundred femtosecond [14], but all these methods have the same disadvantage of requiring extra complex and expensive equipment, such as an extra light source, modulator and high-frequency electrical signal generator, etc. The feed-back locking methods of phase noise and timing jitter reduction have been investigated in passively MLLs [17-19] and in application in WDM transmission [20]. The results of 3dB RF linewidth reduction from 187 kHz to 1.9 kHz corresponding to a pulse-to-pulse jitter reduction to 23 fs have been obtained in a 40 GHz InAs/GaAs QD MLL [9, 21]. Although the method of optical external cavity self-injection feedback is a powerful technique for linewidth and pulse jitter reduction, this technology still need a precise alignment with external cavity and the performance sensitive to the external mode-locking conditions.

We have previously demonstrated InAs/InP QD MLLs with pulse repetition rates from 10 GHz to 437 GHz and a total output power up to 50 mW per facet at room temperature [22-31]. We have recently demonstrated femtosecond timing jitter in InAs/InP QD C-band SSP MLLs with surface ridge waveguide structure by both analysis of the Lorentzian linewidth of the first harmonic RF PSD [32] and optical linewidth [33]. In this paper, we carry out an investigation of various properties of 25 GHz C-band QD Febry-Perot (F-P) MLL based SSP OFC with buried heterostructure (BH) waveguide to extend the study in [34]. Firstly, we theoretically analyze timing jitter and its measured methods for a QD F-P MLL, which is a critically important parameter for high-speed network applications. Then we give a full description of laser fabrication and performance characterization. Furthermore, we compare the measured results of RIN, phase noise and timing jitters from QD F-P MLL with BH structure to a conventional ridge structure. The results show the performance is significantly improved by using BH structures as the laser gain waveguide. To our knowledge, this is the first time in the literatures for making these comparisons. Lastly, we report on application of the 25 GHz QD F-P MLL based OFC for fiber-wireless integrated 5G new radio fronthaul systems with 16-QAM modulated data formats and optical heterodyne detection using both signal modulated signal and LO reference from the same OFC. Those results postulate a complete perspective on these semiconductor QD MLLs as OFC sources for the purpose of being employed in mm-wave RoF transmission systems.

2. Theory of Timing Jitter

Generally, the noise effects in a semiconductor mode-locked laser are mainly from the amplitude, the central optical frequency, the pulse frequency spacing, and the optical phase, but the broadening of the mode lineshape in the passively MLL is dominated by the contributions of optical phase noise and pulse timing fluctuations [35, 36]. The phase and timing fluctuations in each mode are affected by amplified spontaneous emission noise going through a random walk process [37]. Therefore, the timing jitter exhibits a diffusion-like behavior. If $\Delta t_r(t)$ expresses the timing fluctuations in the mode position at time t, the timing jitter σ can be described by a Gaussian random process with mean = 0 and total variance $\sigma = \langle|\Delta t_r(t)|^2\rangle = Dt$, where D is the timing jitter diffusion constant. Then phase fluctuation follows the behavior $\Delta\theta(t) = 2\pi f_0 \Delta t_r(t)$, where f_0 is the center frequency or repetition rate. From analyzing the complex electric field of a semiconductor passively MLL, considering only the effects of phase and timing fluctuations, the complex optical field is [36]

$$E(t) = \sum_{n=-\infty}^{\infty} A[t - n\Delta t(n)] e^{-j[2\pi f_0 (t - nT_0) + \Delta\theta(n) + \phi(n)]}, \quad (1)$$

where $A(n)$, $\Delta t(n)$, $f_0(n)$, $\Delta\theta(n)$ and $\phi(n)$ are respectively the mode envelope, timing fluctuations, the center frequency, phase noise, and static phase of the n_{th} longitudinal mode. T_0 is the repetition period and $f_0 = 1/T_0$. Following [38], the optical spectrum can be calculated by taking the electric field

autocorrelation function and Fourier transform. A set of Lorentzian modes with frequencies f_n and the FWHM linewidths Δf_n compose the optical spectrum as

$$S(\upsilon) \sim \frac{|\hat{A}(f-f_0)|^2}{\pi} \sum_{n=-\infty}^{\infty} \frac{\Delta f_n}{(f-f_n)^2+\Delta {f_n}^2}, \quad (2)$$

where $\hat{A}$ is the Fourier transform of the mode envelope. The quantum limited optical phase noise and timing jitter random walk fluctuations induce the Lorentzian mode shape in all the longitudinal modes [35]. The FWHM optical mode linewidth is [39]

$$\Delta f_n = \Delta f_{min} + 2\pi f_0^2 D(n-n_{min})^2, \quad (3)$$

where n_{min} is the mode number corresponding to the minimum linewidth Δf_{min}, Δf_{min} would be the linewidth for all the modes if there was no timing fluctuations.

In the same way, the spectrum of the laser intensity, or more commonly called the radiofrequency (RF) spectrum of beating note, can be calculated as a set of Lorentzians with the FWHM linewidth of m_{th} harmonic expressed by Δf_{RFm} [36]

$$S_{RF}(\upsilon) \sim \frac{1}{\pi} \sum_{n=-\infty}^{\infty} \frac{\Delta f_{RFm}}{(f-mf_0)^2+\Delta f_{RFm}^2} \quad (4)$$

It is found that the RF spectrum is consist of a sum of Lorentzian modes centered at mf_0 with each harmonics corresponds to the beating between a pair of modes separated by m-1 modes in the optical spectrum. At any given value of m, each harmonics will have integer m^2 proportional multiple to the 1st harmonic linewidth and related to D given by [39]

$$\Delta f_{RFm} = \Delta f_{RF1} m^2 = 2\pi {f_0}^2 D m^2 \quad (5)$$

From the coefficients of Eq. (5), the relationship between the first harmonic RF spectrum linewidth and timing jitter diffusion constant D can be extracted and are given by

$$\Delta f_{RF1} = 2\pi f_0^2 D \quad (6)$$

RF spectrum could be possibly perturbed by the amplitude noise as in the case of actively mode-locked laser [40]. Higher harmonics of the photocurrent could be used to distinguish between phase noise and amplitude noise. However, in passively MLL, the amplitude noise is dominated by the phase, consequently using any different order of the harmonics has no influence on the RF linewidth [41] as shown in Eq. (5).

From Eq. (3) and Eq. (6), for a passively MLL, the optical mode linewidth Δf_n and the 1st RF harmonic linewidth Δf_{RF1} are related by way of

$$\Delta f_n = \Delta f_{min} + \Delta f_{RF1}(n-n_{min})^2 \quad (7)$$

Eq. (7) shows that the first harmonic RF linewidth Δf_{RF1} of the semiconductor passively MLL can be estimated from measuring the optical linewidth, i.e. optical phase noise, of each longitudinal mode and performing a parabolic fit as a function of mode number.

From the well-known method developed by von der Linde [40] for actively mode-locked lasers, phase noise spectrum $L(f)$ is equal to the normalized RF power spectral density (PSD) $P(f)$ as shown in Fig. 1 (a) in one Hz bandwidth, and is given by

$$L(f) = \frac{P(f-f_0)}{RBW * P_{tot}}, \quad (8)$$

where f_0 and P_{tot} are the carrier peak frequency and total integrated power of the RF PSD, respectively, and RBW is the resolution bandwidth used in the RF spectrum analyzer. Drzewietzki, *et al.* [42] verified that this phase noise estimation method is only valid for passively MLLs at frequency offsets well above the carrier peak linewidth. Fig. 1 (b) shows a typical phase noise spectrum $L(f)$ for a passively MLLs, where f_1, f_2, f_3, and f_4 indicate the frequency boundaries of the different noise mechanisms with various slopes, such as flicker frequency modulation ($1/f^3$), white flicker frequency noise ($1/f^2$), flicker phase modulation ($1/f^1$), and white phase noise ($1/f^0$), respectively [43]. The A_{12}, A_{23}, A_{34} and A_{45} represent corresponding noise areas of the different noise mechanisms.

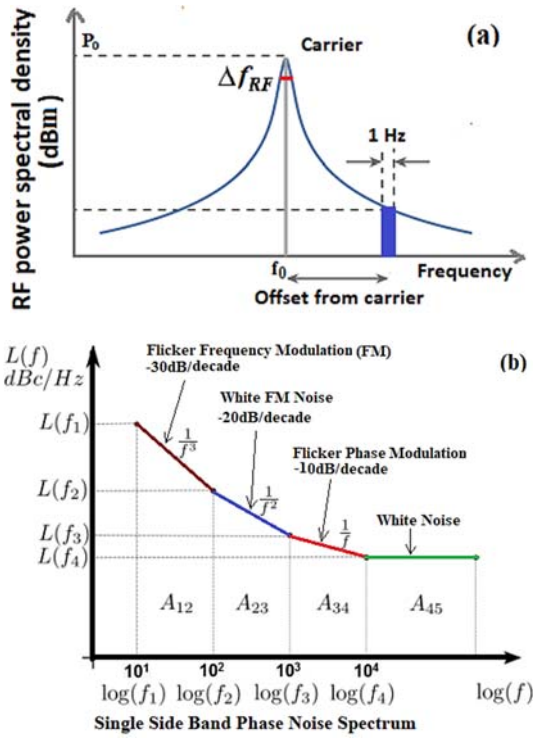

Fig. 1. (a) The 1st homonic RF power spectral density (PSD) with showing FWHM bandwidth and central frequency. (b) A single side band phase noise spectrum with showing the different noise mechanisms with frequency related various slopes.

For the case of an F-P, i.e. passively, mode-locked semiconductor laser, especially for the active region in a laser diode consists of quantum dot or dash (QD) structures is investigated in this work. It is shown that due to material nonlinearities and saturated absorber in the gain area, the phase correlation of the optical longitudinal modes can take place resulting in a four wave mixing process and in passively mode-locking [44]. The common integrated root-mean-square (RMS) time jitter, also called the pulse to clock timing jitter, can be obtained from integration of the single side band phase noise spectrum as shown in Eq. (9) and Fig. 1 (b) by

$$\sigma_{int} = \frac{1}{2\pi f_0}\sqrt{2\int_{f_{low}}^{f_{high}} L(f)df} = \frac{1}{2\pi f_0}\sqrt{2(A12 + A23 + A34 + A45)}, \quad (9)$$

where f_{high} and f_{low} are the upper and lower integration frequencies, respectively, in the interested range and A_{12}, A_{23}, A_{34}, A_{45} are corresponding to the areas of flicker frequency modulation, white flicker frequency noise, flicker phase modulation and white phase noise, respectively [43], as shown in Fig. 1 (b). As pointed out in [42], this phase noise estimation method is only valid for passively MLLs at frequency offsets well above the carrier peak linewidth.

A time jitter estimation method was proposed specifically for a semiconductor passively MLL [41]. The properties of intrinsic phase noise from relatively broadband spontaneous emission in the PML laser leads to a Lorenzian shaped PSD of photocurrent RF phase noise. Study of the linewidth of the first harmonic of photocurrent RF can provide a simple and appropriate way to characterize the timing jitter of a semiconductor PML laser. According to reference paper [41], for a high repetition rate passively MLL, as expressed in f_0, the pulse to pulse RMS timing jitter σ_{ptp} can be expressed as:

$$\sigma_{ptp} = \frac{1}{f_0}\sqrt{\frac{\Delta f_{RF}}{2\pi f_0}}, \quad (10)$$

where Δf_{RF} is the full width at half maximum (FWHM) Lorentzian linewidth of the first harmonic of RF power spectral density. By measuring the first harmonic of photocurrent RF PSD of a semiconductor PML laser and fitting the peak with a Lorentzian function, time jitters can be estimated. From Eq. (10), it is noticed that for a certain repetition rate f_0, the pulse to pulse timing jitters of a semiconductor PML laser are proportional to square root of the Lorentzian linewidth of the RF PSD of the laser. Therefore, the FWHM of the radio-frequency (RF) beat note from a semiconductor MLL determines the level of phase coherence between the modes of the optical frequency comb (OFC).

From Eq. (7), the first harmonic RF linewidth Δf_{RF1} can be estimated by measuring the optical phase noise of each longitudinal mode and performing a parabolic fit as a function of mode number. Therefore, the pulse to pulse jitter can be estimated from optical phase noise measurements by parabolic curve fitting as shown in Eq. (10). This method does not require a direct measurement of the RF PSD which for a high repetition rate laser necessitates the use of a high speed photodetector. Therefore, this method is not restricted to measuring lasers with repetition rates below ~100 GHz.

3. Material Grown and Decice Fabrication

InAs QD is grown initially with an InP buffer following by lattice matched InGaAsP (1.15Q), 1.15 μm PL peak at 300 K, by chemical beam epitaxy (CBE) on exactly (001) oriented n-type InP substrates, as shown in Fig. 2 (a). The laser active region consists of five stacked layers of InAs quantum dashes as shown a cross-sectional scanning electron microscopy (SEM) imaging in Fig. 2 (b). The five InAs dash layers were deposited followed by a 25 s growth interruption for each layer to allow the In to diffuse on the surface and form dashes. The average QD density in each active layer was around $3.5 \times 10^{10} cm^{-2}$.

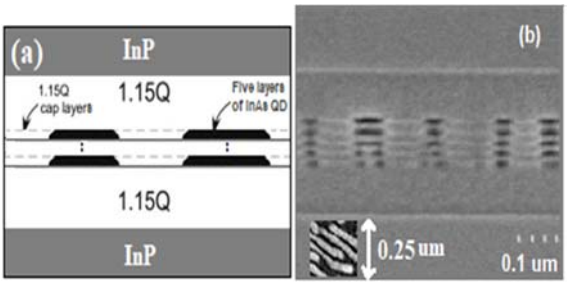

Fig. 2. (a) Schematic diagram of a InAs quantum dash (QD) grown structure; (b) SEM images of the front cross-sectional of the five quantum dashes layers. Inset: the top view of a QD layer in the active region for gain material of the QD MLL.

The each dash layers is then capped with 1.15Q barrier layer and finally capped with 1.15Q and InP. The waveduide core was surrounded by n- and p- type InP cladding layers. This core structure provides both carrier and optical confinement in the active region emitting in C-band wavelength range. Inset in Fig. 1 (b) shows SEM imaging of the top view of the QD layers. More detailed information of the QD material growth is contained in [44]. Two laser structures of buried hetero-structure (BH) and conventional surface ridge (SR) waveguides are fabricated with the same processing environment in this study.

The QD buried heterostructure (BH) MLL is an InP-based p-n blocked BH Fabry-Perot (FP) laser. Fig. 3 (a) shows a schematic of the cross-section of the laser.

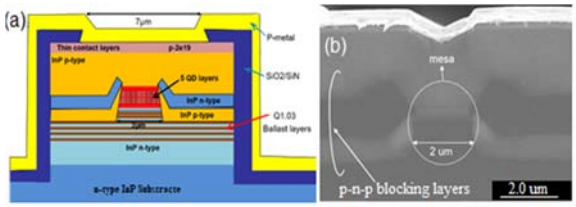

Fig. 3. (a) A schematic front cross-sectional diagram, and (b) SEM images of the fully processed F-P QD MLL with a buried BH waveguide structure.

The laser structure is comprised of a 170 nm thick InGaAsP waveguide core with 10 nm InGaAs P (1.15Q) barriers embedding five stacked layers of InAs QDs as the active gain region surrounded by n- and p- type InP cladding layers. After growing the laser core, a 2 µm wide waveguide mesa was created by etching through the 1.15Q waveguide core followed by the selective area epitaxy overgrowing of pnp blocking layer structure to confine current and light to the waveguide mesa. Then after removing the selective area dielectric mask, the final p-type InP cladding and contact layers were grown. Both facets of the laser were left uncoated. A SEM image of the front cross-section of a fully fabricated QD BH MLL laser is shown in Fig. 3 (b).

The cleaved laser chip with desired cavity length is mounted onto a commercially available Aluminum Nitride (AlN) chip-on-carrier (CoC) with two gold (Au) electroplated contacts to provide mechanical support and electrical connection to the laser chip, where the bottom contact provides a cathode connection through Eutectic Gold Tin (AuSn) and the top contact provides the corresponding anode connection through wire-bonding. For the experimental characterization of the QD MLL and to reduce the power driving noise and environment temperature frustration, the CoC is placed on a copper block with a thermoelectric cooler (TEC) underneath to maintain an operating temperature range of 16 – 20°C and an ultra-low-noise battery powered laser diode driver controller (LDC) (ILX Lightwave, Model LDC-3722) used to DC bias and the corresponding TEC. The laser output light is collected from its front facet using a collimated lensed polarization maintaining (PM) fiber attached to an isolator for reducing any back-reflections. The position of this fiber is adjustable in three dimensions for coupling the light optimally from the laser cavity.

4. Experimental Results and Discussions

Fig. 4 (a) shows a typical measured laser L-I characteristic curve of a 25 GHz QD F-P MLL with buried heterostructure structure at 19 °C. It can be seen that the laser threshold current is at around 50 mA and provides an average output power up to 50 mW at around 450 mA. By comparing the L-I curve of BH laser to that of ridge laser as shown in Fig. 4 (a), it is observed that differential efficiency of BH laser is higher than ridge laser, so the output power is higher for BH laser when the driving current larger than 250 mA. The laser output spectrum is characterized using an optical spectrum analyzer (Anritsu, Model AQ6317B) with a resolution of 0.01 nm at driving current of around 423 mA as shown in Fig. 4 (b). The laser operates in the shorter part of the C band with its central wavelength of around 1531 nm and 6-dB optical bandwidth of around 9 nm providing about 47 highly coherent optical channels.

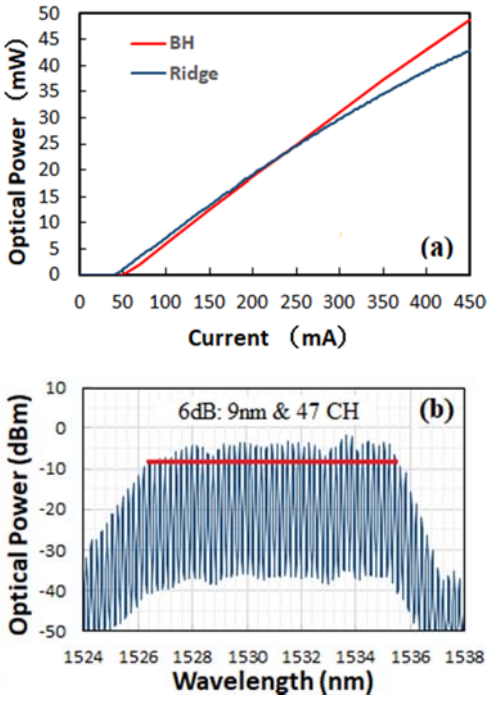

Fig. 4. Measured (a) L-I characteristics and (b) optical spectrum of a 25 GHz QD BH F-P MLL.

To verify the noise performance of the 25GHz QD BH MLL, typical RIN and frequency noise spectra from an individual comb line are charactrizated as shown in Fig. 5 (a) and (b), respectively. For comparison purpose, the noise performances from a 25 GHz QD MLL with surface ridge structure are measured in the same experimental conditions as shown in Fig. 5 as well. RIN is measured using Agilent N4371A measurement system. Although RIN does not usually play an important role in the coherent communications, since balanced receivers suppress the RIN influence of both the carrier and the LO. However, due to the comb modes constantly exchange energy amongst each other caused by mode partition noise [45], the RIN of the individual comb lines usually is high and cannot be neglected, especially in the application in an optical heterodyne based RoF fronthaul wireless network where a single optical receiver is used. From measured RIN spectra over the frequency range of 10 MHz to 10 GHz shown in Fig. 5 (a), we achieve an integrated average RIN value of -143.3 dB/Hz for the QD BH MLL, which is about 6 dB lower than that of the QD MLL with ridge

structure. Such low RIN values are attributed to the characteristics of QD material inside the laser cavity with very low mode partition noise in the BH waveguide active region. Fig. 5 (b) shows measured frequency noise and it can be seen that the frequency noise is at least 10 times lower in the case of BH QD MLL in the high frequency range compared with ridge structure laser.

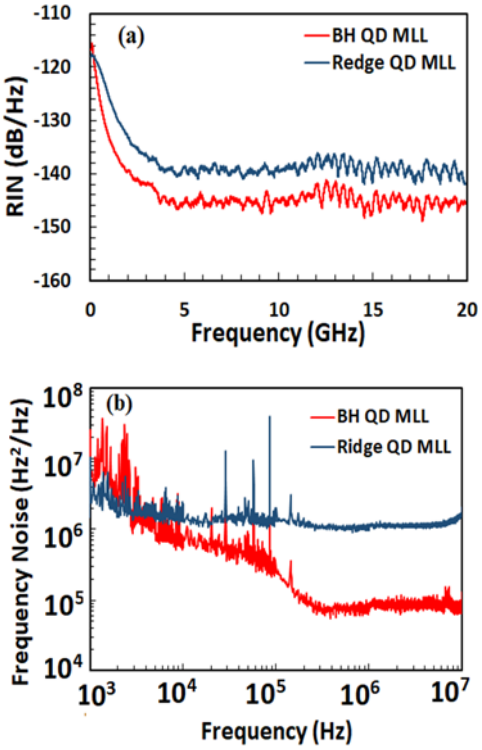

Fig. 5. Measured single channel RIN (a) and frequency noise spectra (b) from a 25 GHz QD BH F-P MLL in comparison to that obtained from a QD ridge F-P MLL with the same repetition rate in the same measured conditions.

To characterize the phase noise performance of the laser, selected individual optical channels covering the spectrum of the laser in the C-band are filtered out using an optical band pass filter. The optical spectral linewidth, i.e. phase noise, for some of the selected channels from 1526.4 nm to 1535.8 nm (covering 47 modes) is estimated from the measured optical frequency noise spectrum using an automated laser linewidth / phase noise measurement system (OEWaves Inc. OE4000) as shown in Fig. 6 (a). The performance is characterized for QD ridge MLL under the same measured conditions. It is indicated as shown in Fig. 6 (a) that the measured phase noise for the QD BH MLL is in between 0.13 MHz to 0.46 MHz, which is much lower than the measured phase noise from 0.97 MHz to 5.5 MHz for laser in SR structure.

For analysis of the timing jitter from optical phase noise, the measured curves of phase noise vs. mode channel number are parabolic fitted using Eq. (7). The fitting results of $\Delta\upsilon_{nim}$, n_{nim} and $\Delta\upsilon_{RF1}$ for both lasers are listed in Table 1 for comparison.

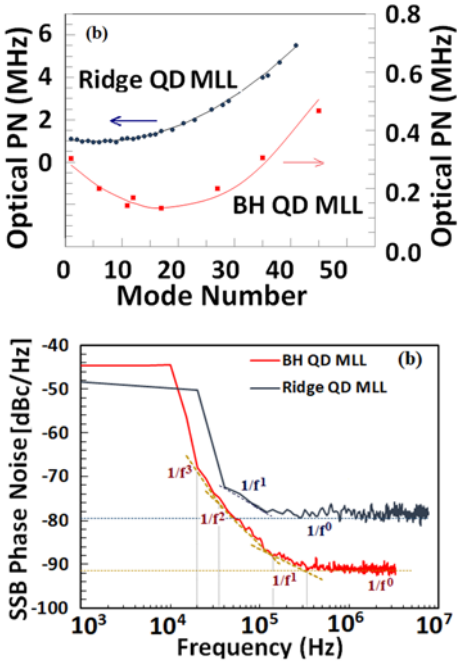

Fig. 6. Measured (a) optical phase noise vs. laser mode number, and (b) single side-band (SSB) phase noise spectrum obtained from a 25 GHz QD BH MLL in comparison with that from ridge QD MLL.

Table 1. Lists of Parabolic fitted results of the minimum optical linewidths.

Laser Structure	*Fit from Phase noise vs. Mode #*			*Pulsed Timing Jitter (fs)*	*Integrated Timing Jitter (ps)*
	$\Delta\upsilon_{nim}$ *(MHz)*	n_{nim}	$\Delta\upsilon_{RF1}$ *(kHz)*		
Ridge	0.968	5.6	3.57	6.03	1.90
BH	0.133	18.1	0.512	2.28	0.48

Lists of Parabolic fitted results of the minimum optical linewidths, i.e. minimum optical phase noise, $\Delta\upsilon_{nim}$, the minimum mode number n_{nim} and the first harmonic RF spectrum linewidth $\Delta\upsilon_{RF1}$ using Eq. (7) and estimated pulse-to pulse using Eq. (10) and integrated using Eq. (9) timing jitters for the 25 GHz QD F-P MLL with both buried heterostructure and surface ridge structures.

The minimum linewidths $\Delta\upsilon_{min}$ = 0.133 MHz and the first harmonic RF linewidths $\Delta\upsilon_{RF1}$ = 0.512 kHz are extracted for the lasers with BH structure, which are both about 7 times smaller than that obtained from the laser with surface ridge (SR) structure. The pulse to pulse timing jitter σ_{ptp} = 2.28 fs for the lasers with BH structure are estimated from $\Delta\upsilon_{RF1}$ using Eq. (10) as shown in Table 1, which is about 3 times lower than that of laser with SR structure. Furthermore, to investigate the integrated timing jitter performance, a SSB phase noise spectrum is calculated from measured RF PSD by Eq. (9) using a high speed IR photodetector and PXA signal analyzer (Keysight Technologies Model N9030A) at the settings of RBW = 10 kHz as shown in Fig. 6 (b) for the

25 GHz QD F-P MLLs in the both cases of BH and SR structures. The calculated integrated timing jitter of 1.90 and 0.48 ps are obtained for QD MLLs with SR and BH structures respectively. The integrated timing jitter is reduced about 4 times in the case of fabricated MLL with BH structure as compared with SR structure. From Fig. 6 (b), for the F-P QD MLL with BH structure, it is observed that the four typical noise types, flicker frequency modulation, white flicker frequency noise, flicker phase modulation and white phase noise, demonstrated predicted down tendency with slopes of $1/f^3$, $1/f^2$, $1/f$ and $1/f^0$, respectively, as discussed in Section 2. However, for the F-P QD MLL with SR structure, the noise of flicker phase modulation is dominated and the flicker frequency modulation and white flicker frequency noises are covered by the white phase noise. The white phase noise of the F-P QD MLL with BH structure is 12 dB lower than that from the F-P QD MLL with SR structure. This is perhaps the reason that the performance of RIN, phase noise and timing jitter of laser with BH structure is much better than that with SR structure.

5. Application

There is a strong connection between the timing jitter of an OFC and the data bandwidth capability since the timing jitter is strongly related to the optical phase noise of each individual longitudinal mode. Both the modulation data rate and the number (N) of the higher-order data modulation format, i.e. PAM-N or N-QAM, are inversely proportional to the phase noise of each individual laser channel. If the phase noise or the timing jitter is smaller, a higher modulation data rate and a larger N can be achieved. The performance of InAs/InP QD F-P BH MLL is evaluated in system experiments by realizing photonics-assisted RoF wireless data transmission links in this study. The experimental setup comprised of central office (CO), remote ratio unit (RRU) and wireless receiver as shown in Fig. 7. More detailed information of the system setup is contained in [46]. In this experimental setup, a typical 5G fronthaul with centralized
radio access network is emulated. Two optical channels (λ_1 and λ_2) from the OFC laser source are used, where λ_1 serves as a modulated data channel and λ_2 as an optical local oscillator (OLO) for remote heterodyne up-conversion. The remote optical heterodyne of the two optical channels up-converts the baseband data signal with Gigabit signal rate to the desired RF carrier signal in optical domain at the remote radio unit (RRU) without using any RF electrical LO.

In the CO, the C-band QD F-P MLL with BH structure is used as an optical source, which is biased at around 423 mA and maintained at 19 °C by using a high stable laser driving controller. The multi-wavelength output of QD BH MLL is connected to a 3 dB PM optical coupler (OC_1) through a two stage PM isolator, to avoid any back reflections caused by subsequent equipment, followed by two tunable optical band pass filters ($OBPF_1$ and $OBPF_2$) in each output of OC_1.

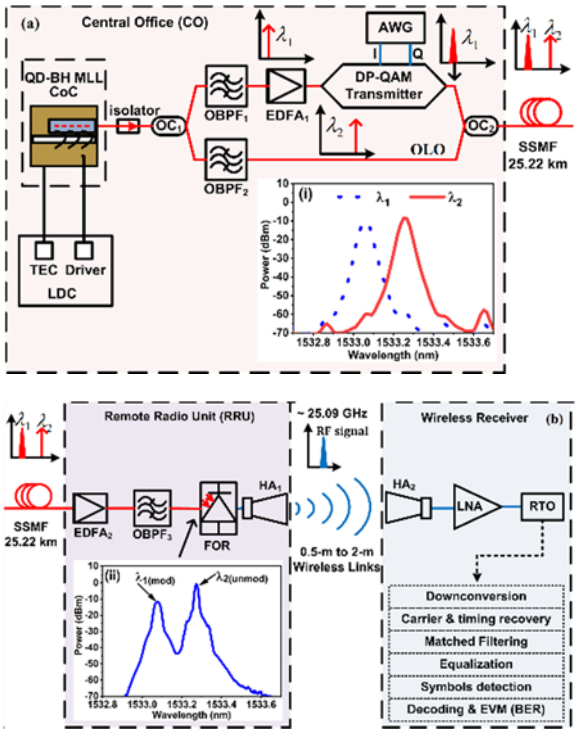

Fig. 7. Schematic of the experimental setups of Central Office (a) and Remote Radio Unit and Wireless Receiver (b) for photonics-assisted RoF RF signal generation, data transmission and detection using two optical channels (data channel λ_1 and optical LO λ_2) from an InAs/InP QD F-P MLL with BH structure. Where: OC = optical coupler; OBPF = optical band pass filter; EDFA = erbium-doped fiber amplifier; AWG = arbitrary waveform generator; OLO = optical local oscillator; FOR = fiber-optic receiver; HA = Horn antenna; LNA = low noise amplifier; RTO = real-time oscilloscope.

Two adjacent optical channels are select from the MLL by the two OBPFs; one for data transmission and another as an optical LO for photonic up-conversion at the RRU, spacing at the RF carrier frequency near to the center of the standard 3GPP 5G NR (a global standard for 5G wireless interface) frequency band n258 (24.25 to 27.5 GHz) of frequency range 2 (FR2). The wavelength of the two selected optical channels are at 1533.044 nm (λ_1) and 1533.240 nm (λ_2), respectively, which are filtered out from the free running optical comb spectrum obtained from the QD BH MLL cavity without using any controlled feedback locking mechanism. It is noteworthy that the QD MLL is a promising source since the selection of the optical channels is flexible and it can be used to generate RF signals in higher frequency bands of mm-wave spectrum including K-band, V-band, W-band and even THz range depending on the channels spacing selection. After boosting the power of optical data channel (λ_1) by an erbium-doped fiber amplifier

($EDFA_1$), it is modulated with 16-QAM digital baseband signals having a symbol rate of 4-GBaud by employing two channels of in-phase (I) and quadrature (Q) from a dual polarization (DP) QAM optical transmitter system (SHF 46215B DP-QAM). The two channels' baseband signals are generated electronically using an arbitrary waveform generator (AWG) (Keysight Technologies, Model M9502A) with a pseudo random binary sequence (PRBS) pattern of 2^{-11}-1 bits and a root raised cosine filter with roll-off factor of 0.35 is also applied for pulse shaping. The second optical channel (λ_2) is used as a supplementary channel to provide OLO for heterodyne RF carrier signal generation at the RRU. The modulated and unmodulated optical signals are then combined in a 3 dB OC_2 and transmitted over a 25 km SSMF to the RRU.

In the RRU, the received optical signal is amplified by $EDFA_2$ followed by $OBPF_3$ to filter out the effect of amplified spontaneous emission (ASE) noise and other optical components. These two optical signals are then beat together on a 38-GHz bandwidth fiber-optic receiver (FOR) (New Focus model 1474-A) to generate the 16 Gb/s (4-GBaud×16-QAM) modulated RF carrier signal at 25 GHz. The FOR is directly attached to a 17 dBi Horn antenna (WR-34) with a 20-33 GHz bandwidth that transmits the generated 4-GBaud RF data signal over 0.5 m to 2 m free-space indoor wireless distance. After wireless transmission, the RF signal is then received by another identical aligned Horn antenna and amplified by a low noise amplifier (LNA) before capturing into a real-time oscilloscope (RTO) for processing. The signal is captured and coherently detected in real-time by using a 33-GHz bandwidth and 100 GSa/s speed Tektronix DPO73304SX oscilloscope with vector signal analysis software (SignalVu). This process involves several digital signal processing (DSP) steps before the signal is demodulated, which include signal down conversion, carrier and symbol locking, RRC matched filtering to recover the baseband IQ data and to minimize inter-symbol interference (ISI), adaptive equalization to compensate for linear distortions, symbols detection and data decoding to calculate the error vector magnitude (EVM) and bit error rate (BER). Finally, the system performance is evaluated by analyzing EVM and BER of the received decoded 16-QAM 4-GBaud (16-Gb/s) data signals. The BER is calculated from the measured EVM values based on the EVM and BER relationship derived in [47].

The performance of EVM and BER is evaluated in a proof-of-concept end-to-end fiber-wireless integrated system experiment by generating, transmitting and detecting broadband RoF wireless signals in the downlink in real-time. The EVM and BER below the standard limit of 12.5 % [48] and FEC requirement of 3.8×10^{-3}, respectively, are successfully achieved in the photonics-assisted wireless system with remote frequency up-conversion and detection of 4-GBaud 16-QAM baseband data signals over 25 km SSMF and 0.5 m to 2 m free-space indoor wireless RF links. Fig. 8 (a) shows the calculated BER and measured EVM as a function of RF link distance at a fixed received optical power of around 2 dBm. It can be seen that for all the RoF wireless links, a BER of well below the standard FEC is achieved. Moreover, Fig. 8 (b) and Fig. 8 (c) shows the corresponding constellation and eye diagrams of the received 16-QAM data signals with the measured RMS EVM values of 6.62 %, 6.92 %, 7.72 % and 8.43 % for RF wireless link distance of 0.5 m, 1 m, 1.5 m and 2 m, respectively. In addition, Fig. 8 (c) shows the clear and open eye diagrams for the corresponding 4-Gbaud received signals for all of the RF wireless links. These results indicate that low noise monolithic integrated InAs/InP F-P QD BH MLL with broadband flat spectra having multiple highly coherent optical channels and ultra-low timing jitters described in this paper is a promising optical source for potential applications in high speed and high capacity 5G fiber-wireless integrated systems.

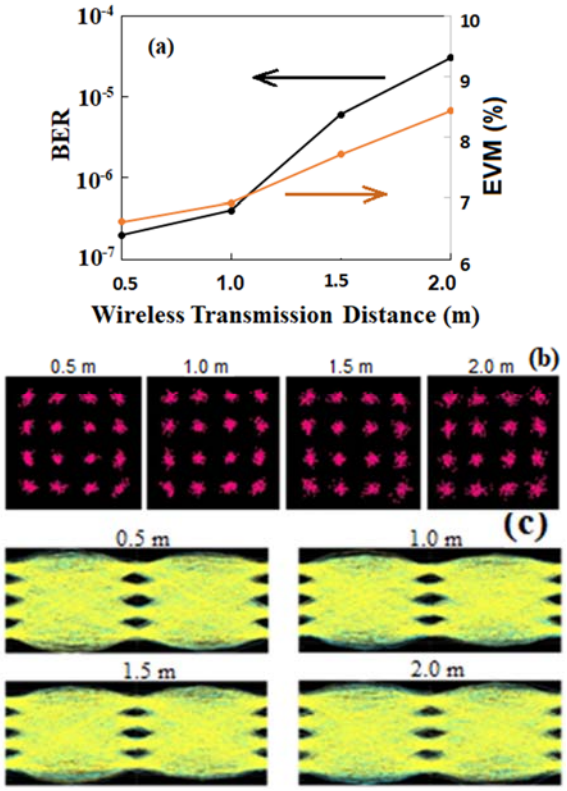

Fig. 8. Experimental transmission performance of the F-P QD BH MLL in photonics-assisted 16-Gb/s (4-Gbaud×16 QAM) wireless links at 25 GHz 5G NR over 0.5 m to 2 m RF link distance through 25 km SSMF (a) obtained BER (left axis) and EVM (right axis); (b) 16-QAM constellations and (c) corresponding eye diagrams observed for 4-Gbaud 16-QAM signals after 0.5 m, 1 m, 1.5 m and 2 m wireless links.

6. Conclusions

We have developed, experimentally characterized and demonstrated monolithically integrated 25 GHz C-band InAs/InP QD Febra-Perio mode-locked laser

(MLL) based optical frequency comb (OFC). Measured method of timing jitter is studied through a direct measurement of the first harmonic RF PSD using a fast photodiode and from optical phase noise measurements. The results from the two method are matched very well, while the optical method has an advantage of not limited by the speed of the photodetector and suitable for extremely high-speed OFC where a photodiode could be a limiting factor. Moreover, growth of InAs/InP QD gain materials and fabrications of F-P MLL with buried heterostructure (BH) waveguides are described. The laser performance is evaluated and compared with the laser with conventional ridge waveguide. An low integrated average RIN value (-143.3 dB/Hz) is achieved for a filtered individual channel of the QD BH MLL, which is about 6 dB lower than that of the QD MLL with ridge structure. Optical phase noise less than 466 kHz is achieved over the comb wavelength range and it is at least 10 times lower than the measured results of a QD MLL with ridge structure. Moreover, pulse to pulse timing jitter values of 2.28 fs is achieved for the QD BH MLL, which is about 3 times lower than that obtained for the laser with ridge structure. Furthermore, by investigating its integrated timing jitter performance from the single side band phase noise spectrum, the levels of flicker phase modulation noise and the white phase noise are all about 12 dB lower than that with surface ridge structure. This could be the possible reason that the performance of laser with BH structure are much better than that with surface ridge structure. In addition, by using the QDash BH MLL, we have successfully demonstrated 16-Gb/s (4-GBaud×16-QAM) RoF-based optical heterodyne RF wireless signal delivery at 25 GHz with a total of 25 km SSMF and up to 2 m wireless links achieving EVM and BER well below the standard requirements. The results indicate that monolithically integrated semiconductor InAs/InP QDash BH MLL with simple and compact design providing large number of highly correlated optical channels with low noise and high power performance can be a cost-efficient and promising solution for high capacity and high speed RoF-based fronthaul systems of 5G and beyond wireless networks.

Acknowledgements

The authors would like to acknowledge supports from National Challenge Program “High Throughput and Secure Networks (HTSN)” in National Research Council (NRC) Canada.

References

[1]. Y. Kim, H. Lee, P. Hwang, R. Patro, J. Lee, W. Roh, K. Cheun, Feasibility of Mobile Cellular Communications at Millimeter Wave Frequency, in *IEEE Journal of Selected Topics in Signal Processing*, Vol. 10, Issue 3, April 2016, pp. 589-599.

[2]. R. Proietti, *et al*., Elastic optical networking by dynamic optical arbitrary waveform generation and measurement, *Journal of Optical Communications and Networking*, Vol. 8, Issue 7, July 2016, pp. A171-A179.

[3]. Juned N. Kemal, Joerg Pfeifle, Pablo Marin-Palomo, M. Deseada Gutierrez Pascual, Stefan Wolf, Frank Smyth, Wolfgang Freude, Christian Koos, Multi-wavelength coherent transmission using an optical frequency comb as a local oscillator, *Opt. Express*, Vol. 24, Issue 22, 2016, pp. 25432-25445.

[4]. Cosimo Calo, Quantum dot based mode locked lasers for optical frequency combs. Networking and Internet Architecture, *Institut National des Télécommunications*, 2014.

[5]. F. Lelarge, B. Dagens, J. Renaudier, R. Brenot, A. Accard, F. van Dijk, D. Make, O. Le Gouezigou, J. G. Provost, F. Poingt, J. Landreau, O. Drisse, E. Derouin, B. Rousseau, F. Pommereau, G. H. Duan, Recent advances on InAs/InP quantum dash based semiconductor lasers and optical amplifiers operating at 1.55 μm, *IEEE Journal of Selected Topics in Quantum Electronics*, Vol. 13, Issue 1, 2007, pp. 111–124.

[6]. R. Rosales, K. Merghem, C. Calo, G. Bouwmans, I. Krestnikov, A. Martinez, A. Ramdane, Optical pulse generation in single section InAs/GaAs quantum dot edge emitting lasers under continuous wave operation, *Applied Physics Letters*, Vol. 101, Issue 22, 2012, 221113.

[7]. P. Bardella, L. L. Columbo, M. Gioannini, Self-generation of optical frequency comb in single section quantum dot Fabry-Perot lasers: a theoretical study, *Opt. Express*, Vol. 25, Issue 21, 2017, pp. 26234-26252.

[8]. W. W. Chow, S. Liu, Z. Zhang, J. E. Bowers, M. Sargent III, Multimode description of self-mode locking in a single-section quantum-dot laser, *Opt. Express*, Vol. 28, Issue 4, 2020, pp. 5317-5330.

[9]. D. Arsenijevi´c, M. Kleinert, D. Bimberg, Breakthroughs in photonics 2013: Passive mode-locking of quantum-dot lasers, *IEEE Photon. J.,* Vol. 6, Issue 2, Apr. 2014, Art. No. 0700306.

[10]. K. Merghem, A. Akrout, A. Martinez, G. Aubin, A. Ramdane, F. Lelarge, G. Duan, Pulse generation at 346 GHz using a passively mode locked quantum-dash-based laser at 1.55 μm, *Appl. Phys. Lett.*, Vol. 94, Issue 2, 2009, 021107.

[11]. D. Eliyahu, R. A. Salvatore, A. Yariv, Noise characterization of a pulse train generated by actively mode-locked lasers, *J. Opt. Soc. Amer. B*, Vol. 13, Issue 7, 1996, pp. 1619-1626.

[12]. Fiol G., Arsenijević D., Bimberg D., Vladimirov A. G., Wolfrum M., Viktorov E. A., Mandel P., Hybrid mode-locking in a 40 GHz monolithic quantum dot laser, *Appl. Phy. Lett.*, Vol. 96, Issue 1, 2010, 011104.

[13]. Arkhipov R., Pimenov A., Radziunas M., Rachinskii D., Vladimirov A. G., Arsenijević D., Bimberg D., Hybrid mode locking in semiconductor lasers: simulations, analysis, and experiments, *IEEE J. Quantum Electron.*, Vol. 19, Issue 4, 2013, pp. 1100208-1100208.

[14]. Habruseva T., Arsenijević D., Kleinert M., Bimberg D., Huyet G., Hegarty S. P., Optimum phase noise reduction and repetition rate tuning in quantum-dot mode-locked lasers, *Appl. Phy. Lett.*, Vol. 104, Issue 2, 2014, 021112.

[15]. Arkhipov R. M., Habruseva T., Pimenov A., Radziunas M., Hegarty S. P., Huyet G., Vladimirov A.

G, Semiconductor mode-locked lasers with coherent dual-mode optical injection: simulations, analysis, and experiment, *JOSA B*, Vol. 33, Issue 3, 2016, pp. 351-359.

[16]. Fiol G., Kleinert M., Arsenijević D., Bimberg D., 1.3 μm range 40 GHz quantum-dot mode-locked laser under external continuous wave light injection or optical feedback, *Semicond. Sci. Technol.,* Vol. 26, 2011, 014006.

[17]. Otto C., Lüdge K., Vladimirov A. G., Wolfrum M., Schöll E., Delay-induced dynamics and jitter reduction of passively mode-locked semiconductor lasers subject to optical feedback, *New Journal of Physics,* Vol. 14, Issue 11, 2012, 113033.

[18]. Jaurigue L., Pimenov A., Rachinskii D., Schöll E., Lüdge K., Vladimirov A. G., Timing jitter of passively-mode-locked semiconductor lasers subject to optical feedback: A semi-analytic approach, *Physical Review A,* Vol. 92, Issue 5, 2015, 053807.

[19]. Nikiforov O., Jaurigue L., Drzewietzki L., Lüdge K., Breuer S., Experimental demonstration of change of dynamical properties of a passively mode-locked semiconductor laser subject to dual optical feedback by dual full delay-range tuning, *Optics Express,* Vol. 24, Issue 13, 2016, pp. 14301-14310.

[20]. Aubin G., Brenot R., Calo C., Freude W., Kemal J., Koos C., Lelarge F., Marin-Palomo P., Merghem K., Ramdane A., Randel S., 32QAM WDM transmission using a Quantum-Dash Passively Mode-Locked Laser with resonant feedback, *Optical Fiber Communication Conference Postdeadline Papers*, Th5C.3, 2017.

[21]. Arsenijević D., Kleinert M., Bimberg D., Phase noise and jitter reduction by optical feedback on passively mode-locked quantum-dot lasers, *Applied Physics Letters,* Vol. 103, Issue 23, 2013, 231101.

[22]. Z. G. Lu, J. R. Liu, S. Raymond, P. J. Poole, P. J. Barrios, D. Poitras, 312-fs pulse generation from a passive C-band InAs/InP quantum dot mode-locked laser, *Optics Express*, Vol. 16, 2008, pp. 10835-10840.

[23]. J. R. Liu, Z. G. Lu, S. Raymond, P. J. Poole, P. J. Barrios, G. Pakulski, D. Poitras, G. Z. Xiao, Z. Y. Zhang, Uniform 90-channel multiwavelength InAs/InGaAsP quantum dot laser, *Electron. Lett*., Vol. 43, 2007, pp. 458-460.

[24]. J. R. Liu, Z. G. Lu, S. Raymond, P. J. Poole, P. J. Barrios, D. Poitras, Dual-wavelength 92.5 GHz self-mode-locked InP-based quantum dot laser, *Optics Letters*, Vol. 33, 2008, pp. 1702-1704.

[25]. Z. G. Lu, J. R. Liu, P. J. Poole, S. Raymond, P. J. Barrios, D. Poitras, G. Pakulski, P. Grant, D. Roy-Guay, An L-band monolithic InAs/InP quantum dot mode-locked laser with femtosecond pulses, *Optics Express*, Vol. 17, 2009, pp. 13609–13614.

[26]. Z. G. Lu, J. R. Liu, P. J. Poole, Z. J. Jiao, P. J. Barrios, D. Poitras, J. Caballero, X. P. Zhang, Ultra-high repetition rate InAs/InP quantum dot mode-locked lasers, *Optics Communications*, Vol. 284, 2011, pp. 2323-2326.

[27]. Z. J. Jiao, J. R. Liu, Z. G. Lu, X. P. Zhang, P. J. Poole, P. J. Barrios, D. Poitras, A C-Band InAs/InP Quantum Dot Semiconductor Mode-Locked Laser Emitting 403-GHz Repetition Rate Pulses, *IEEE Photonics Technol. Lett*., Vol. 23, Issue 9, 2011, pp. 543-545.

[28]. Z. G. Lu, J. R. Liu, P. J. Poole, C. Y. Song, J. Weber, L. Mao, S. D. Chang, H. P. Ding, P. J. Barrios, D. Poitras S. Janz, Integrated InAs/InP quantum-dot coherence comb lasers, in *Proc. SPIE Photonics West*, San Francisco, CA, USA, 2017, pp. 10107-10118.

[29]. Z. G. Lu, J. R. Liu, C. Y. Song, J. Weber, Y. Mao, S. D. Chang, H. P. Ding, P. J. Poole, P. J. Barrios, D. Poitras, S. Janz, M. O'Sullivan, High performance InAs/InP quantum dot 34.462-GHz C-band coherent comb laser module, *Opt. Express*, Vol. 26, Issue 2, 2018, pp. 2160-2167.

[30]. Z. G. Lu, J. R. Liu, P. J. Poole, Y. Mao, J. Weber, G. C. Liu, P. Barrio, InAs/InP Quantum Dash Semiconductor Coherent Comb Lasers and their Applications in Optical Networks, *Journal of Lightwave Technology*, Vol. 39, Issue 12, 2021, pp. 3751-3760.

[31]. Lu Z. G., Liu J. R., Poole P. J., Song C. Y., Chang S. D., Ultra-narrow linewidth quantum dot coherent comb lasers with self-injection feedback locking, *Optics Express,* Vol. 26, Issue 9, 2018, pp. 11909-11914.

[32]. Y. Mao, J. Liu, Z. Lu, C. Song, P. J. Poole, Ultra-low Timing Jitter of Quantum Dash Semiconductor Comb Lasers with Self-injection Feedback Locking, *IEEE J. of Select. Topics in Quantum Electronics*, Vol. 25, Issue 6, Nov. 2019, 1900607.

[33]. Y. Mao, Z. G. Lu, J. R. Liu, P. J. Poole, G. C. Liu, Pulse Timing Jitter Estimated From Optical Phase Noise In Mode-lock Semiconductor Quantum Dash Lasers, *J. of Lightwave Technology*, Vol. 38, Issue 17, 2020, pp. 4787-4793.

[34]. Y. Mao, K. Zeb, Z. G. Lu, J. R. Liu, E. Liu, P. Poole, M. Rahim, G. Pakulski, P. Barrios, W. Jiang, X. Zhang, Study of Phase Noise and Timing Jitter in InAs/InP Quantum Dash Mode-locked Lasers for Application in 5G RoF Wireless Networks, in *Proc. of the 4th International Conference on Optics, Photonics and Lasers (OPAL'2021)*, Corfu, Greece, 13-15 October 2021, pp. 33-35.

[35]. Y. Takushima, H. Sotobayashi, M. E. Grein, E. P. Ippen, H. A. Haus, Linewidth of mode combs of passively and actively mode-locked semiconductor laser diodes, *Proc. of SPIE*, Vol. 5595, 2004, pp. 213–227.

[36]. T. Habruseva, S. O'Donoghue, N. Rebrova, F. Kéfélian, S. P. Hegarty, G. Huyet, Optical linewidth of a passively mode-locked semiconductor laser, *Opt. Lett.,* Vol. 34, Issue 21, 2009, pp. 3307-3309.

[37]. J. P. Tourrenc, A. Akrout, K. Merghem, A. Martinez, F. Lelarge, A. Shen, G. H. Duan, A. Ramdane, Experimental investigation of the timing jitter in self-pulsating quantum-dash lasers operating at 1.55 μm, *Opt. Express*, Vol. 16, Issue 22, 2008, pp. 17706–17713.

[38]. F. X. Kärtner, U. Morgner, T. Schibli, R. Ell, H. A. Haus, J. G. Fujimoto, E. P. Ippen, Few-cycle pulses directly from a laser, *Top. Appl. Phys*., Vol. 95, 2004, pp. 73-136.

[39]. R. Rosales, K. Merghem, A. Martinez, F. Lelarge, A.Accard, A. Ramdane, Timing jitter from the optical spectrum in semiconductor passively mode locked lasers, *Optics Express*, Vol. 20, Issue 8, 2012, pp. 9151-9160.

[40]. D. von der Linde, Characterization of the noise in continuously operating modelocked lasers, *Appl. Phys. B*, Vol. 39, Issue 4, 1986, pp. 201–217.

[41]. F. Kefelian, S. O'Donoghue, M. T. Todaro, J. G. McInerney, G. Huyet, RF linewidth in monolithic passively mode-locked semiconductor laser, *IEEE Photon. Technol. Lett.*, Vol. 20, Issue 16, 2008, pp. 1405–140.

[42]. L. Drzewietzki, S. Breuer, W. Elsaßer, Timing jitter reduction of passively mode-locked semiconductor

lasers by self- and external-injection: Numerical description and experiments, *Opt. Express*, Vol. 21, Issue 13, 2013, pp. 16142–1616.
[43]. S. Latkowski, Radio frequency and terahertz signals generated by passively modelocked semiconductor lasers, PhD Dissertation, *Dublin City University,* Dublin, Ireland, 2010.
[44]. P. J. Poole, K. Kaminska, P. Barrios, Z. G. Lu, J. R. Liu, Growth of InAs/InP-based quantum dots for 1.55 μm laser applications, *J. Cryst. Growth*, Vol. 311, Issue 6, 2009, pp. 1482-1486.
[45]. Y. Ben M'Sallem, *et al.*, Quantum-Dash Mode-Locked Laser as a Source for 56-Gb/s DQPSK Modulation in WDM Multicast Applications, in *IEEE Photonics Technology Letters*, Vol. 23, Issue 7, 2011, pp. 453-455.
[46]. K. Zeb, Z. G. Lu, J. R. Liu, Y. Mao, G. C. Liu, P. J. Poole, M. Rahim, G. Pakulski, P. Barrios, W. Jiang, J. Zhang, InAs/InP quantum dash buried heterostructure mode-locked laser for High Capacity Fiber-wireless Integrated 5G New Radio Fronthaul Systems, *Optics Express*, Vol. 29, Issue 11, 2021, pp. 16164-16174.
[47]. R. Schmogrow, B. Nebendahl, M. Winter, A. Jopstern, D. Hillerkuss, S. Koenig, J. Meyer, M. Dreschmann, H. Huebner, C. Koos, J. Becker, W. Freude, J. Leuthold, Error vector magnitude as a performance measure for advanced modulation formats, *IEEE Photon. Technol. Lett.*, Vol. 24, Issue 1, 2012, pp. 61–63.
[48]. ETSI TS 138.101-2 V15.3.0, User equipment (UE) radio transmission and reception, Tech. Rep., Part 2: Range 2 standalone, (3GPP TS 38.101-2 V15.3.0 Release 15), 2018.